Maximizing absorption and scattering by spherical nanoparticles

Yezekyan, Torgom; Nerkararyan, Khachatur V.; Bozhevolnyi, Sergey I.

Published in:
Optics Letters

DOI:
10.1364/OL.387046

Publication date:
2020

Document version:
Final published version

Optics Letters

Maximizing absorption and scattering by spherical nanoparticles

TORGOM YEZEKYAN,[1] KHACHATUR V. NERKARARYAN,[2] AND SERGEY I. BOZHEVOLNYI[1,*]

[1]Centre for Nano Optics, University of Southern Denmark, Campusvej 55, DK-5230 Odense M, Denmark
[2]Department of Radiophysics, Yerevan State University, A. Manoogian 1, Yerevan, 0025, Armenia
*Corresponding author: seib@mci.sdu.dk

Received 2 January 2020; revised 5 February 2020; accepted 7 February 2020; posted 10 February 2020 (Doc. ID 387046); published 12 March 2020

The absorption and scattering resonances of metal nanostructures are often assumed to be defined b y the same condition of localized surface plasmon resonance. Using an electrostatic approximation, we demonstrate that the absorption and scattering cross sections of spherical nanoparticles reach their maxima at different wavelengths, which in turn differ from that defined by the Fröhlich condition (FC). These deviations from the FC originate from and are proportional to the material absorption. Our results provide the design guidelines for maximizing absorption and scattering of spherical nanoparticles and are thus of special importance for applications where the efficiency of radiation absorption or scattering is crucial.

https://doi.org/10.1364/OL.387046

The interaction of light with metal nanostructures excites collective electron oscillations coupled to local electromagnetic fields, i.e., surface plasmons. Under certain conditions, these excitations become resonant producing localized surface plasmon resonances (LSPRs), which result in strongly enhanced and localized electromagnetic fields causing in turn enhanced radiation absorption and scattering [1]. Absorption and scattering resonances have historically been used for producing colored glasses by embedding metal nanoparticles in glass [2]. More recently, metal nanoparticles started to be considered and exploited as local nano-sources of heat, which can remotely be controlled by externally incident light, thus opening an exciting perspective to control thermal-induced phenomena at the nanoscale [3–5]. Such a powerful and flexible photothermal scheme attracted a great deal of interest due to various applications, including photothermal therapeutics [3], drug release [6], thermal-optical data storage [7], solar thermal energy harvesting [8,9], and optoelectronic devices [10].

Considering materials used for nanoparticles, apart from well-known gold and silver, several conductive nitrides such as titanium nitride (TiN) and zirconium nitride (ZiN) have recently been introduced as plasmonic materials [11–13]. The fact that their optical losses are higher than those of noble metals, along with very high melting temperatures, makes these materials beneficial for the applications involving the broadband sunlight absorption and efficient conversion [12]. Spherical and cylindrical core-shell structures made of poor metals have also been investigated as broadband absorbers for the same purposes [14,15].

Spherical nanoparticles are probably the simplest and best understood nanostructures supporting LSPRs. Nevertheless, even for these simple structures, it is usually implicitly assumed that the local field enhancement as well as the absorption and scattering cross sections are resonantly enhanced at the LSPR wavelength determined by the Fröhlich condition (FC) [1,16–18]. Interestingly and importantly, it has previously been noticed that there is a spectral shift between the near- and far-field LSPR responses. It has also been revealed that this shift is a universal phenomenon, with its value increasing when increasing the imaginary part of the nanostructure permittivity [19–21].

In general, LSPRs (as with any other resonances) are determined by solutions of homogeneous equations, i.e., in the absence of the external driving field, that provide a set of resonant wavelengths and field distributions (modes). At the same time, electromagnetic (far and near) fields, absorption, scattering, and extinction represent different responses, which are driven by the external field and described by inhomogeneous equations and, as such, should be expected to exhibit different spectra peaking at different wavelengths. The corresponding solutions, however, include a set of resonant fields (modes), whose contribution becomes progressively dominant when the system damping decreases. Therefore, it should be expected that all aforementioned differences would disappear in the limit of negligibly small damping. Applications of plasmonic nanostructures based on the radiation absorption, however, require the opposite, i.e., large damping, encouraging one to examine closer differences in the LSPR and absorption (and scattering) responses.

Here, using the electrostatic approximation, we analyze in detail the responses of homogenous nanospheres and spherical core-shell nanostructures and demonstrate that spectral positions of absorption and scattering maxima are completely different, being also different from the FC. We show that these differences originate from and are proportional to the material dispersion and absorption. We also suggest a simple way of estimating the relevant wavelength differences. Our results provide

the design guidelines for maximizing absorption and scattering spherical nanoparticles, and are thus of special importance for applications, where the efficiency of radiation absorption or scattering is crucial.

We begin with briefly reviewing the main formula describing the plane wave scattering by a spherical particle of radius R. Let ε_m and ε_d be the dielectric permittivities of the metal and the surrounding medium, respectively. Within the limits of quasi-static approximation ($R \ll \lambda$, where λ is the wavelength in the medium surrounding the sphere), the dipole moment of a spherical particle is determined by the following expression [22]:

$$\vec{P} = V\chi\vec{E}, \tag{1}$$

where $\vec{E}$ is the incident wave electric field, V is the particle volume, and χ is the electrical polarizability of a spherical particle:

$$\chi = \frac{3}{4\pi}\frac{\varepsilon_m - \varepsilon_d}{\varepsilon_m + 2\varepsilon_d}. \tag{2}$$

Hereafter, we assume that only metal permittivities can have nonzero imaginary parts: $\varepsilon_m = \varepsilon_m' + i\varepsilon_m''$.

Within the electric-dipole approximation the absorption and scattering cross sections of a sphere can then be written in the following forms [22]:

$$\sigma_{\text{abs}} = \frac{8\pi^2}{\lambda} V Im\left(\chi\right), \tag{3a}$$

$$\sigma_{\text{sca}} = \frac{4(2\pi)^5}{3}\frac{V^2}{\lambda^4}|\chi|^2. \tag{3b}$$

As is well known, the absorption cross section is determined by the imaginary part of the polarizability, whereas the scattering cross section is governed by its absolute value squared. The fact that the corresponding expressions are different implies differences in their spectra, including the resonant wavelengths. Moreover, the presence of the (dispersive) nanosphere material in the nominator of the polarizability [Eq. (2)] suggests that the absorption and scattering are maximized at wavelengths that are different from that determined by the FC: $\varepsilon_m' = -2\varepsilon_d$ [1].

Absorption resonance is determined by the factor $Im(\chi) \equiv K_a$, whose equal-magnitude contours in the complex $(\varepsilon_m', \varepsilon_m'')$-plane can be expressed using Eqs. (2) and (3a) as follows:

$$\left(\varepsilon_m' + 2\varepsilon_d\right)^2 + \left(\varepsilon_m'' - \frac{3\varepsilon_d}{2K_a}\right)^2 = \left(\frac{3\varepsilon_d}{2K_a}\right)^2. \tag{4}$$

It is seen that the constant-absorption-factor (CAF) contours represent circles centered along the line $\varepsilon_m' = -2\varepsilon_d$ [Eq. (4)] with radii being inversely proportional to the absorption factor, having a common point, $(-2\varepsilon_d, 0)$, representing a singularity (Fig. 1). Further insight into absorption of nanospheres made of different materials can be obtained by combining the CAF contours with the material dispersion curves mapping $\varepsilon_m''(\varepsilon_m')$, while marking the FC with a vertical line (Fig. 1, the environment permittivity is set to 1). For a given material, the maximum absorption (and the corresponding wavelength) is determined by the point at which the corresponding dispersion curve touches the associated constant-absorption contour, as explicitly indicated in Fig. 1 for titanium (Ti), TiN, and glass-core-Ti-shell nanospheres. Thus, one deduces that the

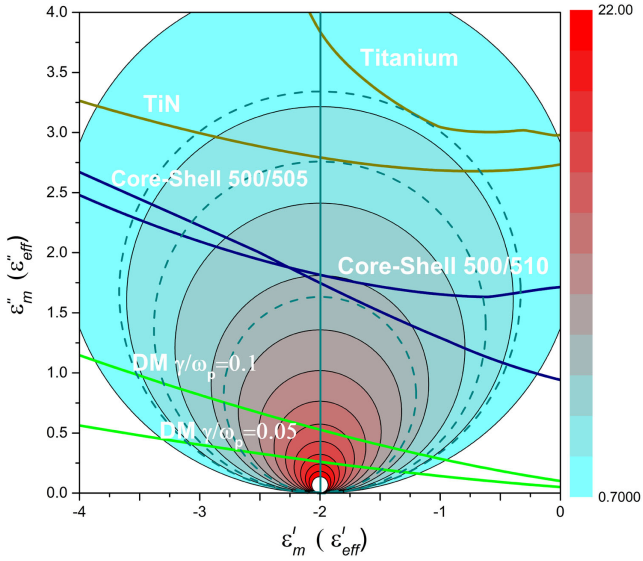

Fig. 1. CAF contours along with the dispersion curves for two DMs with different damping rates γ (green lines) normalized by the plasma frequency ω_p, real metals (dark yellow lines), and core-shell nanospheres (blue lines) described by the effective permittivity [14,23]. Optical parameters for the Ti are taken from Refs. [24,25], and for TiN from Ref. [26]. The FC, $\varepsilon_m' = -2\varepsilon_d$, is marked by a vertical blue line with the dielectric constant of the environment being set to 1. The dashed circles indicate maximum CAF contours for Ti, TiN, and glass-core-Ti-shell nanospheres having the 500 nm radius glass core ($\varepsilon_c = 2.25$) and 5 nm thin shell. 500/505 and 500/510 indicate the ratio R_1/R_2; see the notation after Eq. (5).

deviation of the maximum absorption from the FC increases for larger damping and material dispersion. Somewhat similar behavior was also observed when considering the wavelength shift between resonant near and far fields [19–21].

The electromagnetic responses of homogenous nanospheres are completely determined by the material dispersion, at least in the electrostatic approximation, leaving little room for designing efficient absorbers at specified wavelengths. The situation is very different for spherical core-shell nanoparticles, whose resonances can easily be manipulated by adjusting the ratio between the core radius and the shell thickness [27]. It turns out that there is also more design room with respect to the deviation of the maximum absorption from the FC. Using the electrostatic approximation for spherical core-shell nanoparticles, one obtains the polarizability in the following form [14,15]:

$$\chi_{c-s} = \frac{3}{4\pi}\frac{(1+2\eta\mu)\,\varepsilon_s - (1-\eta\mu)\,\varepsilon_d}{(1+2\eta\mu)\,\varepsilon_s + 2\,(1-\eta\mu)\,\varepsilon_d}, \tag{5}$$

with

$$\eta = \frac{R_1^3}{R_2^3}, \quad \mu = \frac{\varepsilon_c - \varepsilon_s}{\varepsilon_c + 2\varepsilon_s} \quad \text{and} \quad \varepsilon_s = \varepsilon_s' + i\varepsilon_s''.$$

ε_c, ε_s, and ε_d are the dielectric constants of the core, (metallic) shell, and surrounding media, respectively; R_1 and R_2 are the corresponding radii of the core and total core-shell nanosphere. Using the Maxwell–Garnett approach, one can consider sufficiently small core-shell spheres as homogeneous with the following effective permittivity [14,23]:

$$\varepsilon_{\text{eff}} = \varepsilon_s \frac{(\varepsilon_c + 2\varepsilon_s) + 2\eta(\varepsilon_c - \varepsilon_s)}{(\varepsilon_c + 2\varepsilon_s) - \eta(\varepsilon_c - \varepsilon_s)} \equiv \varepsilon'_{\text{eff}} + i\varepsilon''_{\text{eff}}. \quad (6)$$

It has already been emphasized [14] that the real and imaginary parts of the effective permittivity are not independent, while being also dependent on the core-shell geometry, i.e., on the ratio between the core radius and the shell thickness. For this reason, as should be expected, 5 and 10 nm thin shell nanospheres feature different slopes of the dispersion curves, resulting in different wavelength shifts of the absorption maximum from the FC (Fig. 1), even though both are made of the same materials and with the same core radius of 500 nm.

Scattering resonance is determined by the factor $|\chi|^2 \equiv K_s^2$, whose equal-magnitude contours in the complex $(\varepsilon'_m, \varepsilon''_m)$-plane can be expressed using Eqs. (2) and (3b) as follows:

$$\left(\varepsilon'_m + \varepsilon_d \frac{2K_s + 1}{K_s - 1}\right)^2 + \varepsilon''^2_m = \left(\varepsilon_d \frac{3\sqrt{K_s}}{K_s - 1}\right)^2. \quad (7)$$

It is seen that the constant-scattering-factor (CSF) contours represent circles that are centered along the line $\varepsilon''_m = 0$ [Eq. (7)] with radii being inversely proportional to the square root of scattering factor. Importantly, CAF and CSF contours are not concentric (except for extremely large factors: K_a, $K_s \gg 1$, ε_d), implying an interesting possibility of fine tuning, for example, the scattering cross section while maintaining the same absorption cross section, and vice versa. Introducing the material dispersion curves and marking the FC as in the case of absorption allows one to immediately estimate the extent of deviations of the maximum scattering for different nanospheres from the FC (Fig. 2).

One can also notice an interesting phenomenon: for all materials considered in Fig. 1, the absorption maximum is always blueshifted with respect to the FC, while the scattering maximum is blueshifted only for materials with small damping, becoming redshifted in other cases (see Drude metal (DM) examples with other cases in Fig. 3). This difference in deviations from the FC is related to the principal difference in the

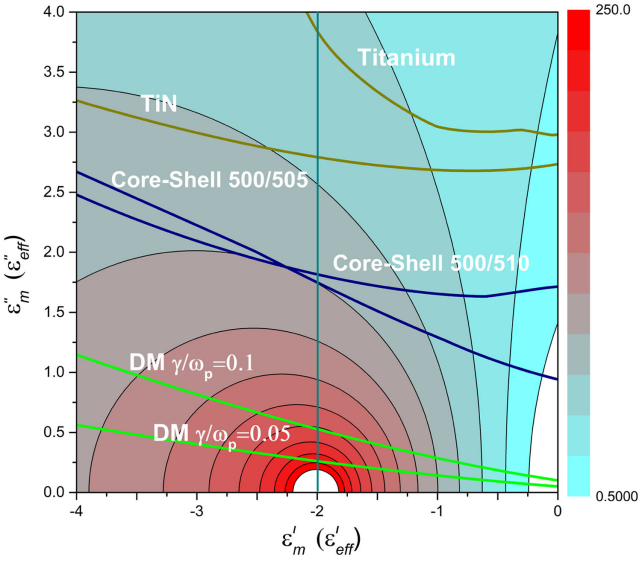

Fig. 2. CSF contours, $|\chi|^2 = \text{const}$, along with the dispersion curves for different materials and core-shell nanospheres. All notations are as in Fig. 1. The dielectric constant of the environment is set to 1.

CAF and CSF contour locations: the CAF contours are centered along the line $\varepsilon'_m = -2\varepsilon_d$, while the CSF contours—along the line $\varepsilon''_m = 0$. Moreover, the rate of changes in the center position of CSF contours (by varying K_s) is considerably smaller than the rate of changes in the contour radius (Fig. 2). The latter means that, for any real material (i.e., with $\varepsilon''_m > 0$), the scattering is maximized for larger permittivity magnitudes than that required by the FC: $\varepsilon'_m(\text{max}) < -2$ (Fig. 2). Consequently, unlike in the absorption case, steeper dispersion curves in the complex $(\varepsilon'_m, \varepsilon''_m)$-plane would not necessarily result in larger deviations in the scattering case. In fact, the dispersion can happen to bring the scattering maximum very close to the FC wavelength [see curves for the Ti nanospheres in Figs. 2 and 3(b)] or even reverse the sign of the displacement. For the same reason, the difference between the absorption and scattering maxima for Ti is smaller than that for TiN nanospheres [Fig. 3(b)], while both the material absorption and slope of the dispersion curve are larger for Ti (Fig. 2).

More detailed information about absorption and scattering behavior (and the deviations of maxima from the FC) can be gleaned from the spectra shown in Fig. 3, in which the FC wavelengths (different for different materials) are explicitly marked by vertical lines. It is now directly seen that the absorption and scattering factors reach their maxima at different wavelengths, which are also different from the FC wavelengths. Note that, for DMs, large damping also means a larger shift between absorption and scattering peaks. In fact, the FC has been formulated for materials with small damping, assuming implicitly that the permittivity imaginary part can be neglected. Still, even for Drude metals with relatively small damping, there appears a noticeable displacement of the maximum absorption [Fig. 3(a)] that might become important for those applications (such as local heating for medical purposes), for which the perfect match between the incident laser wavelength and the maximum absorption wavelength is crucial for achieving the best effect.

We should note that the analyzed CAF and CSF contours deviate from the constant absorption/scattering cross-sectional contours due to the (smooth) wavelength dependencies taken out of the consideration [see Eqs. (3a) and (3b)]. This additional dispersion results in additional wavelength deviations which, however, are small for resonances with appreciable quality factors Q. Assuming a Lorentzian resonance response for the absorption and scattering factors and $Q^2 \gg 1$, the *additional* wavelength deviations can straightforwardly be estimated as $\delta\lambda/\lambda_r \cong -1/(8Q^2)$ and $\delta\lambda/\lambda_r \cong -2/Q^2$ for the absorption and scattering cases, respectively, with λ_r being the resonant wavelength. Note that the wavelength deviation in the absorption case is much smaller than that in the scattering case, because the additional dispersion is weaker (λ^{-1} versus λ^{-4}, respectively).

Finally, in the absorption case (which is very important in many photothermal applications), one can obtain a simple formula for estimating the wavelength difference between the absorption maximum and FC wavelengths. Assuming that the dispersion curve slope is relatively small, it is straightforward to obtain the following estimate for the wavelength difference:

$$\delta\lambda \cong -\frac{d\varepsilon''/d\lambda}{2(d\varepsilon'/d\lambda)^2} \cdot \varepsilon'', \quad (8)$$

where all variables and derivatives are evaluated at the wavelength of the FC. The above formula is found to be accurate

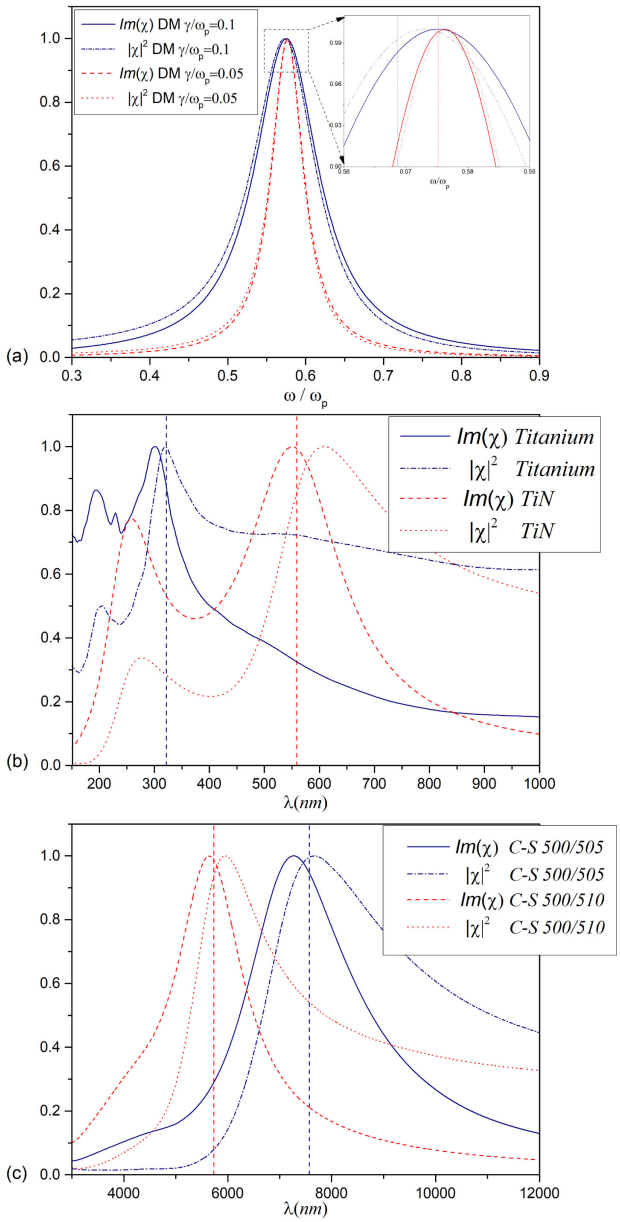

Fig. 3. Wavelength spectra of the absorption and scattering factors for spherical nanoparticles made of different materials: (a) Drude metals, (b) Ti and TiN, and (c) glass-core-Ti-shell nanospheres normalized by their corresponding peak values. The solid and dashed curves correspond to the absorption. The dotted and dashed-dotted curves correspond to the scattering. The vertical lines mark the corresponding FC wavelengths. All notations are otherwise as in Fig. 1.

within 10% for the DM and TiN examples and 20% for core-shell nanospheres, while being quite off for Ti nanospheres.

In conclusion, using an electrostatic approximation, we have analytically considered the absorption and scattering spectra of spherical nanoparticles and demonstrated that the absorption and scattering are maximized at different wavelengths, which in turn differ from the FC wavelength. These differences were argued to originate from and be proportional to the material dispersion and absorption. Our results provide the design guidelines for engineering efficient absorption and scattering of spherical nanoparticles, helping to accurately predict spectral positions of maximum absorption and scattering, and are thus of special importance for applications, where the efficiency of radiation absorption or scattering is crucial.

Funding. H2020 European Research Council (341054); Syddansk Universitet (SDU 2020); Villum Fonden (Award in Technical and Natural Sciences 2019).

Acknowledgment. The authors thank S. Fiedler for useful discussions.

Disclosures. The authors declare no conflicts of interest.

REFERENCES

1. S. A. Maier, *Plasmonics: Fundamentals and Applications* (Springer, 2007).
2. P. Colomban, J. Nano Res. **8**, 109 (2009).
3. L. R. Hirsch, R. J. Stafford, J. A. Bankson, S. R. Sershen, B. Rivera, R. Price, J. D. Hazle, N. J. Halas, and J. L. West, Proc. Natl. Acad. Sci. USA **100**, 13549 (2003).
4. G. Baffou, C. Girard, and R. Quidant, Phys. Rev. Lett. **104**, 136805 (2010).
5. G. Baffou, R. Quidant, and F. J. García De Abajo, ACS Nano **4**, 709 (2010).
6. D. Pissuwan, S. M. Valenzuela, and M. B. Cortie, Trends Biotechnol. **24**, 62 (2006).
7. L. Wang and B. Li, Phys. Rev. Lett. **101**, 267203 (2008).
8. B. J. Lee, K. Park, T. Walsh, and L. Xu, J. Sol. Energy Eng. **134**, 021009 (2012).
9. O. Neumann, A. Urban, J. Day, S. Lal, P. Nordlander, N. Halas, N. Zhou, Y. Tan, J. Wang, W. Xu, Y. Yuan, W. Cai, S. Zhu, and J. Zhu, Nat. Photonics **10**, 393 (2016).
10. L. Vicarelli, M. Vitiello, D. Coquillat, A. Lombardo, A. C. Ferrari, W. Knap, M. Polini, V. Pellegrini, and A. Tredicucci, Nat. Mater. **11**, 865 (2012).
11. N. Kinsey, M. Ferrera, G. V. Naik, V. E. Babicheva, V. M. Shalaev, and A. Boltasseva, Opt. Express **22**, 12238 (2014).
12. S. Ishii, R. P. Sugavaneshwar, and T. Nagao, J. Phys. Chem. C **120**, 2343 (2016).
13. U. Guler, S. Suslov, V. Kildishev Alexander, A. Boltasseva, and M. Shalaev Vladimir, Nanophotonics **4**, 269 (2015).
14. H. A. Parsamyan, K. V. Nerkararyan, and S. I. Bozhevolnyi, J. Opt. Soc. Am. B **36**, 2643 (2019).
15. A. B. Evlyukhin, K. V. Nerkararyan, and S. I. Bozhevolnyi, Opt. Express **27**, 17474 (2019).
16. Y. A. Akimov, W. Koh, S. Sian, and S. Ren, Appl. Phys. Lett. **96**, 073111 (2010).
17. M. Dalarsson, S. Nordebo, D. Sjöberg, and R. Bayford, J. Phys. D **50**, 345401 (2017).
18. S. Nordebo, M. Dalarsson, Y. Ivanenko, D. Sjöberg, and R. Bayford, J. Phys. D **50**, 155401 (2017).
19. J. Zuloaga and P. Nordlander, Nano Lett. **11**, 1280 (2011).
20. F. Moreno, P. Albella, and M. Nieto-Vesperinas, Langmuir **29**, 6715 (2013).
21. C. Menzel, E. Hebestreit, S. Mühlig, C. Rockstuhl, S. Burger, F. Lederer, and T. Pertsch, Opt. Express **22**, 9971 (2014).
22. L. Landau, E. Lifshitz, and L. Pitaevskii, *Eloectrodynamics of Continuous Media* (Oxford, 1984).
23. U. K. Chettiar and N. Engheta, Opt. Express **20**, 22976 (2012).
24. M. A. Ordal, R. J. Bell, R. W. Alexander, L. A. Newquist, and M. R. Querry, Appl. Opt. **27**, 1203 (1988).
25. P. Johnson and R. Christy, Phys. Rev. B **9**, 5056 (1974).
26. G. V. Naik, V. M. Shalaev, and A. Boltasseva, Adv. Mater. **25**, 3264 (2013).
27. R. D. Averitt, S. L. Westcott, and N. J. Halas, J. Opt. Soc. Am. B **16**, 1824 (1999).